Colloid Polym Sci 275:1001–1009 (1997)

ORIGINAL CONTRIBUTION

K.D. Knudsen
J.G. Hernández Cifre
J. García de la Torre

Fracture of flexible polymer chains in dilute solution under transient extensional flow

Received: 17 September 1996
Accepted: 29 May 1997

K.D. Knudsen · J.G. Hernández Cifre
Dr. J. García de la Torre (✉)
Departamento de Quimica Fisica
Facultad de Quimica
Universidad de Murcia
30071 Murcia, Spain

Abstract Applying the technique of Brownian dynamics simulation, we have studied the fracture process of flexible polymer chains when they encounter an extensional flow field of transient character. For this purpose, a mathematical model was made of an experimental device used earlier by other authors to study fracture of polystyrene in dilute solution. The polymer/solvent system studied was a very dilute solution in theta conditions. The polymer molecule was modeled as a FENE bead-spring chain, including a modification to allow for chain fracture. The simulation results showed that the fracture yield depended strongly on flow rate and on molecular weight. We have characterized the molecular-weight dependence of the critical flow rate which is necessary for fracture to occur. The distribution of the resulting fragments is interpreted in terms of the conformation of the chains prior to fracture.

Key words Polymer chain fracture – transient flow – extensional flow – fragment size distribution

Introduction

When polymer chains are subject to strong flow, their shape changes from a random coil to rather extended conformations, and when the flow rate reaches a sufficiently large value, chain fracture can be observed. Extension and fracture in steady elongational flow with a stagnation point has been the subject of a number of experimental [1–4] and theoretical or numerical simulation studies [5–9]. However, in a variety of situations of great practical importance, the chain molecule is exposed to flow for a limited time, during which it experiences a varying extensional rate as it moves down the flow. This type of transient extensional flow occurs when a polymer solution passes through a sudden constriction or a small orifice. Nguyen and Kaush [10, 11] and Reese and Zimm [12] have studied experimentally this situation with dilute solutions of polystyrene and DNA, respectively. With the purpose of comparison with these experiments, and also to confirm some theoretical predictions by Rabin [13, 14] we proposed the simulation of chain extension and fracture in transient flows using the Brownian dynamics simulation technique [15, 16]. In the present work we extend and improve our earlier simulations, employing a more realistic chain model with finitely extensible springs that also allows for spring breakage. We characterize in detail how the flow-rate threshold depends on molecular weight, showing the important influence of hydrodynamic interactions on this dependence. We also visualize, using computer graphics, the three-dimensional shape of the polymer chains, and this is in turn useful to explain the distribution of fracture sites or fragment sizes.

Model and simulation method

Transient flow

In our simulation program (Fig. 1), the polymer chains are submitted to a transient extensional flow developed in

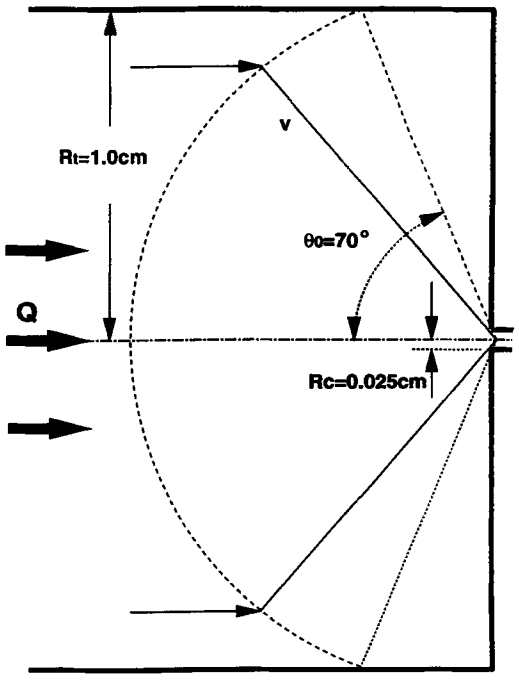

Fig. 1 Outline of the simulated device. The polymer solution first enters a tube with radius R_t on the left-hand side (volumetric flow rate Q), passes through a region with convergent extensional flow, and then enters an orifice with radius R_c

a polymer solution when it passes through a sudden Q, and the velocity along the centerline, v_c, is given by the expression: $Q = (\pi R_t^2/2)v_c$. When the fluid approaches the orifice, the streamlines start to converge. We assume to have convergent flow beginning at a distance from the orifice equal to $\rho_o = R_t/\sin\theta_o$, where R_t is the diameter of the tube as mentioned before and θ_o is the half-angle from the symmetry axis up to which volumetric flow is considered significant [11].

Near the orifice, the velocity along a streamline depends on the distance to the orifice, ρ, being inversely proportional to the square of that distance, as it is commonly assumed for convergent, sink flow:

$$v = v_o\rho_o^2/\rho^2 \,. \tag{1}$$

Here ρ_o equals the length of the convergent flow region and v_o is the velocity in the streamline at the end of the Poiseuille region determined by the instrumental dimensions and the flow rate. We usually restrict our simulations to the particular situation of molecules traveling through the centerline of the device, since this is sufficient for purposes such as the characterization of qualitative aspects, or the determination of power-law exponents for molecular-weight dependences. Thus, v_o is identified with v_c, and can be expressed in terms of the flow rate as $v_o = 2Q/\pi R_t^2$.

The extensional rate is given by the expression $|dv(\rho)/d\rho|$ and equals, in the region of convergent flow, $\varepsilon = 2v_o\rho_o^2/\rho^3$. This parameter is related to the volumetric flow rate as $\varepsilon = (4/\pi)(R_t^2/\rho_o^2)Q/\rho^3$. At a distance from the apex of the conical convergent-flow region, approximately equal to the orifice radius R_c, the extensional flows ends and the flow velocity is constant. In a previous paper [16] we studied a device with a long, thin capillary tube following the orifice. In the present work, we suppose that the constriction is very short, and the device has some outlet or expansion region in which the flow velocity decreases very quickly. This is indeed the case in the Nguyen–Kaush device. We expect that fracture will be negligible beyond the orifice, and thus the simulation can be stopped there.

The numerical values used in our simulations are: tube radius, $R_t = 1.0$ cm; distance at which convergent flow develops is $\rho_o = 1.064$ cm (this flow takes place in a cone of with a semiangle of 70°); orifice radius $R_c = 0.025$ cm. The maximum value of ε (at the boundary where convergent flow ends; see above), for a flow rate of $Q = 0.1$ cm^3/s will be approx. 1.9×10^5 s^{-1}. Changing the value of Q will change the maximum ε-value accordingly.

Polymer model

The polymer/solvent system studied in the present work was a very dilute Θ-solution, for which we choose the specific case of monodisperse polystyrene in cyclohexane at 35 °C, the same as one of the systems used by Nguyen and Kausch [11] in their laboratory experiment. The polymer molecule was in the present study modeled as a bead-spring chain, the springs representing the entropic force of the subchains, and the beads representing the friction between the polymer chain and the surrounding fluid. In order to avoid the unphysical model connected with the linear force law and infinite extensibility of a Gaussian spring, we applied nonlinear (FENE) springs in our bead-spring model of the polystyrene chain. The springs are then governed by the Warner force law [17]

$$F = \frac{-Hq}{1-(q/q_o)^2} \,, \tag{2}$$

where H is the force constant, equal to $3kT/b^2$. Here k is the Boltzmann constant, T the absolute temperature and the parameter b is the root-mean-square spring length (equilibrium spring length). The instantaneous spring length is denoted q. Thus, in the FENE spring the Gaussian force $(-Hq)$ is modified by a term that makes the

extension progressively more difficult as the spring length q approaches the maximum allowable length q_o.

However, in our study we want to allow for fracture of the polystyrene chain, and this is, in principle, not possible with the force law in Eq. (1) since F is infinitely high when q equals q_0. To allow for fracture we have, therefore, introduced a modification in the original FENE model, as described in the following.

From Eq. (1) the potential energy of the FENE spring is found to be

$$V = -\frac{Hq_o^2}{2}\ln[1-(q/q_o)^2] \; . \tag{3}$$

Since fracture of a polystyrene chain is likely to signify breakage of a C–C bond, we decided to consider the spring as fractured when V reaches the dissociation energy of a C–C bond in the polymer chain, taken as 144 kcal/mol [18]. This value of V then corresponds to a critical value q_c of the spring extension and V is considered constant ($F = 0$) for $q > q_c$. It was then important to make sure that this modification does not perturb the main characteristics of the FENE model as represented by the force law in Eq. (1). This was done by forcing the critical spring extension q_c be close to the maximum extension q_o in the FENE model, thus maintaining the nonlinear force law over nearly the whole range of spring extension. Equation (2) can be written as

$$q_o^2 = -\frac{2V}{H}\ln[1-(q/q_o)^2] \; . \tag{4}$$

Now, by deciding upon the value of the ratio q/q_o at the moment of fracture (when $q = q_c$), and inserting the corresponding value of V as mentioned above, together with the value of H, we can thus find from Eq. (14) the corresponding value of q_o and then also the value of q at the moment of fracture (q_c). We have in our model allowed for spring fracture when the spring reaches 93% of the maximum extension q_o in the FENE model ($q_c/q_o = 0.93$), which by means of Eq. (3) leads to $q_o^* = 8.8$ and $q_c^* = 8.2$ (the asterix signifies dimensionless parameters, obtained by dividing lengths by b, the root-mean-square spring length).

Figure 2 illustrates the above-mentioned discusssion by showing the force curve for the spring in our bead-spring model of the polystyrene chain. Since $F_{\text{FENE}}/F_{\text{Gaussian}} = 1/[1-(q/q_o)^2]$ (see Eq. (1)), the spring force in our model at the moment of breakage will be $1/[1-0.93^2] \approx 8$ times higher than in the simple Gaussian spring model, showing that our model represents an improvement with respect to the latter with respect to reduced extensibility of the spring.

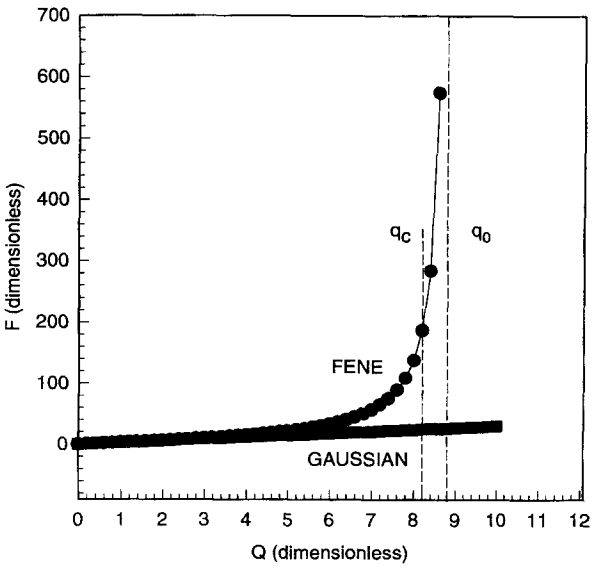

Fig. 2 Relationship between spring force in the applied modified FENE-model and a standard Gaussian spring. The parameter q_o is the maximum extension in the original FENE-model, and q_c is the critical extension at which the spring is considered to brake in our model. The ratio between q_c and q_o is 0.93

We have now discussed the considerations necessary to implement a fracturable FENE-type spring in our model of the polystyrene molecule. To parameterize the polystyrene model, that is, to give the parameters in our model values that are realistic when compared with a real polystyrene molecule, we have started by choosing the molecular weight per bead, M_1, to be 1×10^5. The number of beads, $N = M/M_1$, required for a polymer of about one million in molecular weight is then not too high for the computer simulation. A polymer with molecular weight 2×10^6, will with this assumption be modeled as a 20-bead chain. It can be shown, however, that the final results will not depend on the choice of M_1 provided that N is large enough. Although this number of beads may seem too small, we recall that it yields the correct Gaussian statistics of the end-to-end distance, and it is adequate for describing simple, overall properties such as diffusion coefficients and intrinsic viscosities, and even the behavior in simple flows. For the complex problem studied here, the shortness of the chains may have an unknown effect on the final result. This may be checked in the future, when increased computational power will allow simulation of longer chains.

By combining the experimentally obtained expression (in Θ-solution and at equilibrium) for the relation between the radius of gyration of a flexible polymer and its molecular weight, $\langle S^2 \rangle = C_s M$, with the theoretical expression for $\langle S^2 \rangle$ for a Rouse bead-spring chain [17], $\langle S^2 \rangle = b^2(N^2-1)/6N \approx b^2 N/6$, we obtain an expression for the

Colloid & Polymer Science, Vol. 275, No. 11 (1997)

root-mean-square spring length, $b^2 = 6C_sM_1$. Employing now the experimentally found value [19, 20] for polystyrene in cyclohexane at 35 °C, $C_s = 7.9 \times 10^{-18}$ cm^2 mol/g, we finally end up with a value of 21.7 nm for the equilibrium spring length b.

Brownian dynamics algorithm and simulation procedure

The methodology employed in the present work is essentially the same as in our previous studies [15, 16]. The Brownian Dynamics simulation algorithm is based on that of Ermak and McCammon [21] with a second-order modification [22], which has been shown to give improved calculation efficiency. The displacement of a bead includes the contribution due to solvent flow. When hydrodynamic interaction (HI) between the chain units is taken into account (nonfree draining situation), the Rotne–Prager–Yamakawa interaction tensor [23] is used. For the bead radius σ we used the value $\sigma = 0.256b$, which corresponds to a commonly used value for the hydrodynamic interaction parameter [17], $h^* = 0.25$. For the obtention of quantitative results of real, practical significance, hydrodynamic interaction must be included in theoretical or simulation studies. Anyhow, we have also carried out simulations without HI (free-draining), which are much less expensive in CPU time, and that are still valid for testing the programs and for characterization of qualitative aspects, such as the shape of the fragment size distributions.

The maximum spring force in the FENE springs of our model is considerably higher than that of a simple Gaussian spring (about 8 times, see model section). Therefore, we had to reduce the time step accordingly, at the cost of an increase in computer time. It was necessary to employ a value of Δt as low as 1.5 ns in order to get stable, time-step-independent results.

In the simulations, the polymer chain was initially placed in a random conformation at a distance from the orifice equal to the distance traveled by the chain during a period equal to three times the first Rouse-relaxation time of the molecule. The initial distance from the orifice can then be shown to be calculated from the formula

$$R_{ini} = \left(18 \frac{R_c^2}{\pi R_t^2} \tau Q\right)^{1/3}. \quad (5)$$

For a 20-bead model of polystyrene, which has $\tau = 73\,\mu$s, we have $R_{ini} = 0.076Q^{1/3}$ (R_{ini} in cm and Q in cm^3/s).

In the simulations Brownian trajectories were then simulated for ensembles containing on the order of thousand molecules. While following the trajectory of one molecule, we monitored every spring for fracture ($q > q_c$) at each step in the simulation, registering the molecular weight of the resulting two molecular fragments. Carrying out this for all the chains in the sample, the molecular weight distribution could be evaluated. The initial molecular weight of the polymer was 2×10^6 in most of the work, except for the studies we made about the dependence of critical flow rate upon molecular weight, were we employed molecular weights between 5×10^5 and 2×10^6.

Results and discussion

In Fig. 3 is shown how the fracture yield for chains with different molecular weights was found to depend on the volumetric flow rate (Q). Initially, we ignore hydrodynamic interaction (HI) effects in the simulation. As commented above, thanks to this, the computer time per molecule is much smaller, and this allows for larger samples in the simulation, so that the statistical quality of the results is better. It is seen from the figure that there is a critical flow rate (Q_{crit}), depending on the molecular weight, below which fracture does not occur. The value of Q_{crit} is lowered with increasing molecular weight. This can also be expressed in other words: For a given flow rate Q, chain fracture will occur only for polystyrene chains of sufficiently high molecular weight.

The fracture curves are similar in shape to those obtained by Nguyen and Kausch [11] in their experimental work in polystyrene. However, when we calculate the maximum elongational rate corresponding to each Q-value, we find that in our study the ε_{max} value for a certain fracture yield is higher than those in the work of the above-mentioned authors. It therefore seems that the real polystyrene chains can break more easily than what is presented by our FENE-model of the molecules.

In Fig. 4, we have made a double-logarithmic plot of the relation between the critical flow rate for fracture, extracted from the data in Fig. 3, and the molecular weight of the polymer. We defined the critical flow rate to be the value of Q where the fracture was reduced to a value slightly above zero (operational fracture yield) in order to avoid the problem of finding the zero-crossing in a zone where the data were relatively more noisy than in the rest of the fracture curve. This operational critical yield was set to 8%. The final result is a scaling law of the form, $Q_{crit} \sim M^{-1.49}$. The value of the exponent is significantly lower than that known to exist for fracture in stagnant flow (exponent = −2.0), showing clearly the distinct nature of the transient type of extensional flow. However, it is also significantly different from the exponent close to −1.0 that has been proposed theoretically [13, 14] and observed in some experiments [10] with transient flow. This discrepancy will be discussed in more detail later.

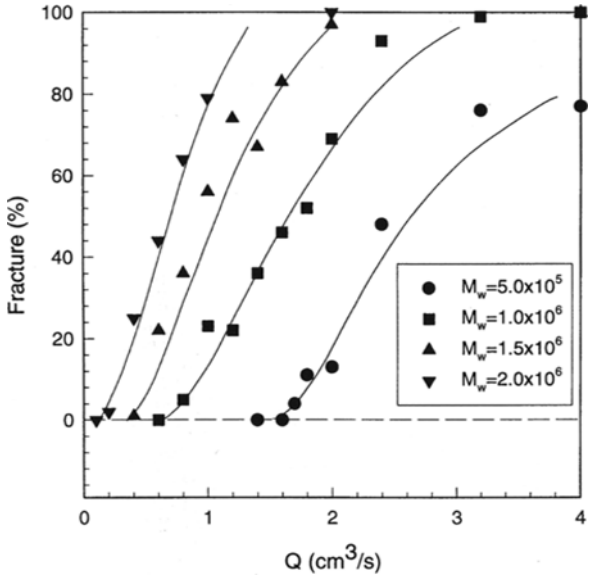

Fig. 3 Simulation results for fracture yield vs. volumetric flow rate for polystyrene of different molecular weights

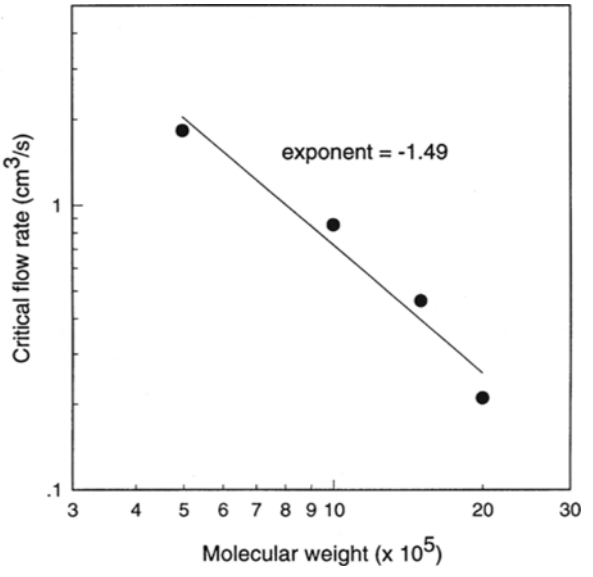

Fig. 4 Critical flow rate for fracture, obtained from the data shown in Fig. 3, plotted double-logarithmically vs. molecular weight M

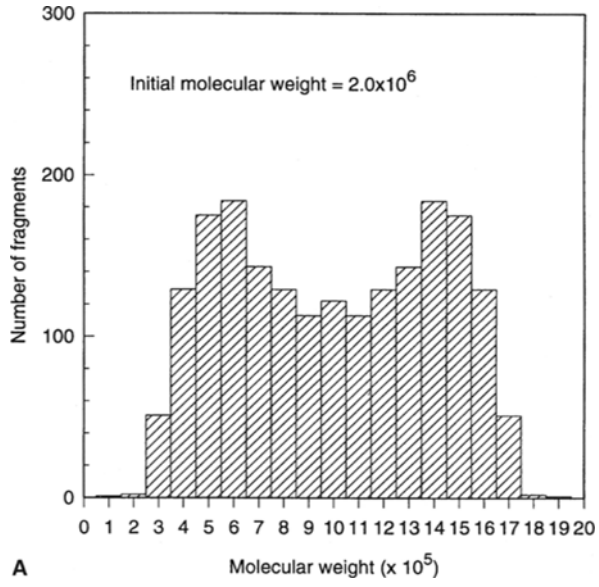

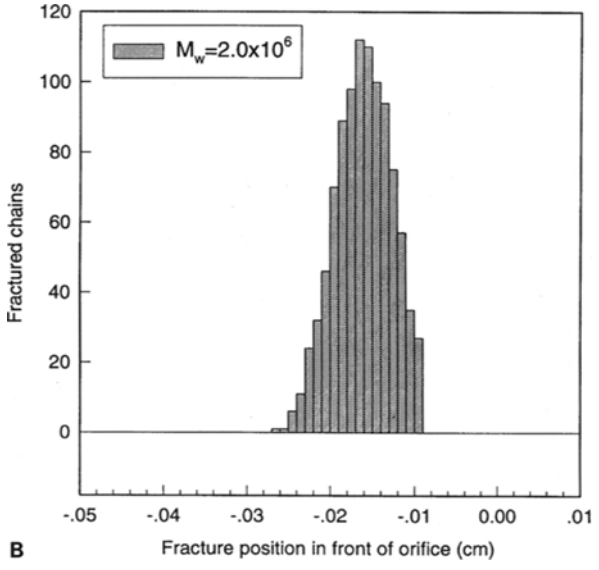

Fig. 5A Molecular weight distribution of polymer fragments after fracture. The molecular weight of the intact chain was 2.0×10^6. The volumetric flow rate used was $Q = 2.0\ \mathrm{cm}^3/\mathrm{s}$. Hydrodynamic interaction was not included (free-draining case). The sample consisted of 1000 chains. **B** Distribution of fracture position (x-coordinate) in front of orifice. Orifice has x-coordinate equal to 0. The molecular weight of the intact chain was 2.0×10^6. Volumetric flow rate used was $Q = 2.0\ \mathrm{cm}^3/\mathrm{s}$. Hydrodynamic interaction was not included (free-draining case). The sample consisted of 1000 chains

In Fig. 5A is shown the molecular weight distribution of fragments after fracture for polystyrene chains of initial molecular weight equal to 2.0×10^6. The volumetric flow rate was $Q = 2.0\ \mathrm{cm}^3/\mathrm{s}$, and the study was performed with free-draining chains. The center of the distribution is situated at a molecular weight of 1.0×10^6, the half of the molecular weight of the intact polystyrene chains. However, the distribution shows the peculiarity of having two peaks around the central molecular weight, suggesting that chain fracture is more likely to occur midway between the chain center and the ends of the chain than in the very center of the chain. An explanation for such a behavior could be that the chain may fold around its center while it

moves towards the orifice, resulting in two "subchains" that each gets accumulated maximum stress in its central region. This kind of distribution has not been observed in laboratory experiments in transient extensional flow, although the computer simulation by Reese and Zimm [12] of DNA fracture in their own instrument at high strains, gives a broad or bimodal distribution similar to ours.

Figure 5B is a histogram showing the distribution of fracture positions in front of the orifice for the same flow rate as used for the results in Fig. 5A. We can see that, for the flow rate in question, the majority of the chains are fractured at a distance of around 0.015 cm from the orifice, which is a distance on the order of the orifice radius (at this distance the elongational rate is about $5 \times 10^5\ s^{-1}$ for the value of $Q = 2\ cm^3/s$ used in Fig. 5). The fracture thus takes place very close to the orifice in comparison with the length of the convergent flow region.

In Figs. 6A and B are shown the distribution of molecular weight fragments and fracture positions for a flow rate of $Q = 10\ cm^3/s$, five times higher than that used for the data shown in Figs. 5A and B. We see from Fig. 6A that the two peaks in the distribution of fragments get more pronounced, suggesting that after a mid-chain folding, the two subchains, due to more complete alignment with the flow lines, accumulate higher stresses in its centers than what was the case with the lower flow rate. As seen from Fig. 6B, with this higher flow rate, as expected, the fracture now takes place earlier, i.e., at a greater distance from the orifice. Most of the chains fracture at a distance of about 0.03 cm from the orifice with this flow rate.

The previous figures showed data obtained for the free-draining (no-HI) case. However, we also studied the fragment distribution and the critical flow rate for fracture taking into account the hydrodynamic interaction between the beads in the chain, having to face the fact that these simulations were considerably more time consuming. We recall the well-known fact in Polymer Physics that the scaling laws for molecular-weight dependence of dynamic properties in solution are correctly obtained only when the HI effect is properly considered. In Fig. 7 is shown a double-logarithmic plot of how the critical flow rate for fracture depends on the molecular weight of the polymer, now for the nonfree draining case (HI). Here we obtain a scaling law of the form $Q_{crit} \sim M^{-1.03}$. The exponent obtained here is much lower than that obtained in the free-draining (no-HI) case, -1.49. Although the no-HI case is not of practical relevance, the comparison between the HI and no-HI cases has still a theoretical interest. The less negative scaling exponent obtained with HI implies that it is more difficult to break a polymer chain due to hydrodynamic interactions. This finding is quite reasonable, since this type of interaction has a shielding effect for concerted motions of the chain, as is the case for the movement in shink flow. Thus, frictional drag at the beads and, therefore, stress accumulation is smaller when HI is considered, and chain fracture requires higher rates.

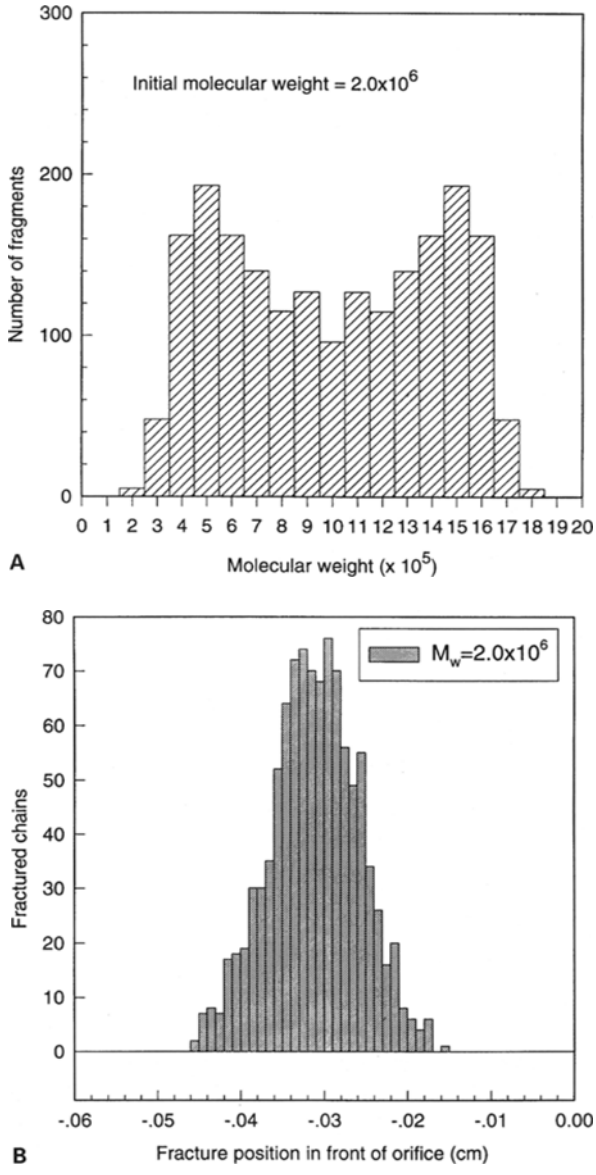

Fig. 6A Molecular weight distribution of polymer fragments after fracture. The molecular weight of the intact chain was 2.0×10^6. The volumetric flow rate used was $Q = 10.0\ cm^3/s$. Hydrodynamic interaction was not included (free-draining case). The sample consisted of 1000 chains. **B** Distribution of fracture position (x-coordinate) in front of orifice. Orifice has x-coordinate equal to 0. The molecular weight of the intact chain was 2.0×10^6. Volumetric flow rate used was $Q = 10.0\ cm^3/s$. Hydrodynamic interaction was not included (free-draining case). The sample consisted of 1000 chains

Our essential result, $Q_{crit} \sim M^{-1.03}$, corresponds well with the exponent found experimentally by Nguyen and Kausch [10], who obtained an exponent equal to -0.95

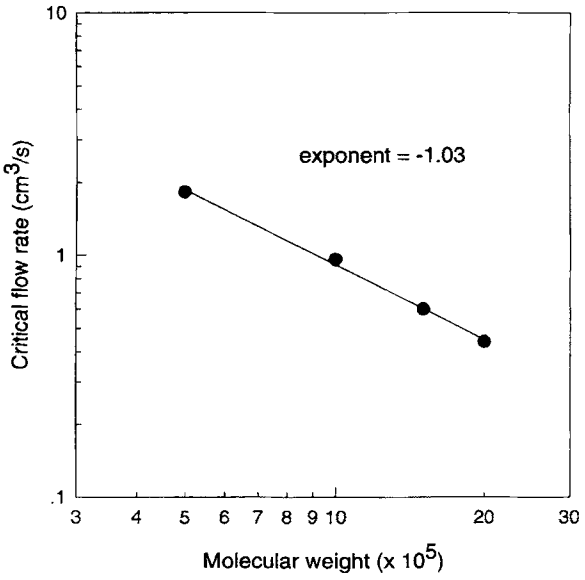

Fig. 7 Critical flow rate for fracture for the nonfree draining case (hydrodynamic interaction included), plotted double-logarithmically vs. molecular weight M

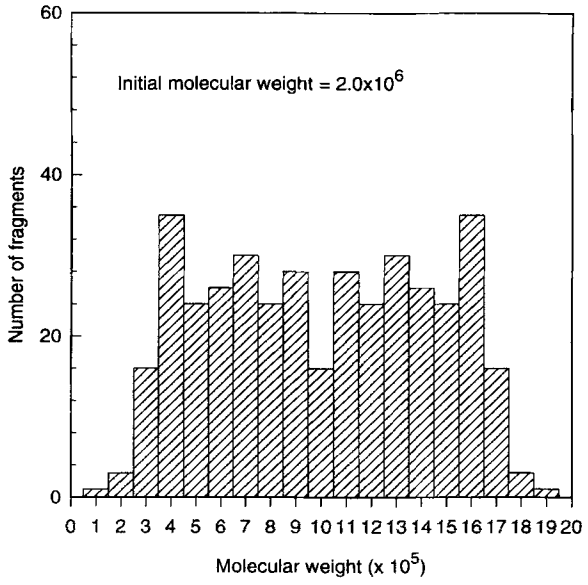

Fig. 8 Molecular weight distribution of polymer fragments after fracture. The molecular weight of the intact chain was 2.0×10^6. The volumetric flow rate used was $Q = 2.0$ cm^3/s. Hydrodynamic interaction was included (non-free draining case). The sample consisted of 200 chains

in their studies on polystyrene fracture. It is also in accordance well with the theoretical study by Rabin [13, 14]. This author argued that the exponent should be in the range -1.0 to -1.2, depending on the goodness of the solvent. In our case, we simulate a system in θ-solution (polystyrene in cyclohexane at 35 °C), which according to the theory then should give an exponent of -1.0, in very good accordance with what we have obtained in this study.

In Fig. 8 is shown the molecular weight distribution of polymer fragments in the nonfree draining case (with HI). Although the statistics is poorer than that in Figs. 5 and 6 due to a reduced number of chains (the computer simulation was very time consuming), it is seen that in this case the distribution is more centered around the half of the initial molecular weight, and that the two peaks observed in Figs. 5A and 6A are reduced in size. This observation, together with the result for the scaling exponent, show that the hydrodynamic interaction is important to take into account in theoretical and numerical studies about fracture in transient flow.

The distribution in Fig. 8 is broader than what one would expect to observe in stagnant, persistently extensional flow [16]. This illustrates that in transient flow the chains do not, on average, obtain the same fully stretched-out conformation before fracture as in stagnant flow.

Figures 9A and B shows pictures of a chain at different stages in the trajectory through the device. In Fig. 9A the flow rate was set low enough ($Q = 0.2$ cm^3/s) that fracture did not occur. The chain starts in a random conformation, unperturbed by the flow (Fig. 9A.1). In the picture the beads have different sizes to illustrate that they do not all lie in the same plane, i.e., the molecule has a finite extension also in the yz-plane (normal to the direction of flow). When the forces induced by the flow field overcome those due to the Brownian motions, the chain starts to stretch out and close to the orifice it has obtained a rather extended conformation (Fig. 9A.2, this picture has been considerably reduced in size for the chain to fit on the page). Having passed the orifice, the chain experiences a reduction in its overall extension (Fig. 9A.3), and as it tumbles down the capillary behind the orifice (Fig. 9A.4), where we have assumed to have a Poiseuille-type of flow pattern, it continuously changes its conformation, having general dimensions considerably smaller than those at the entrance of the orifice.

In Fig. 9B the flow rate was set high enough ($Q = 10$ cm^3/s) that all chains fractured in front of the orifice. From these pictures one can see the reasons for the two fracture peaks observed in the histograms of Figs. 5A and 6A. It seems that the chain possesses the possibility of folding around its center, with the result that it divides itself into two subchains, both of which may be aligned with the flow field. The maximum stress will then be accumulated in the center of each of these subchains, or midway between the center and the extremes of the whole polymer chain. Fracture will in this case occur preferentially here, resulting in the two peaks shown in Figs. 5A

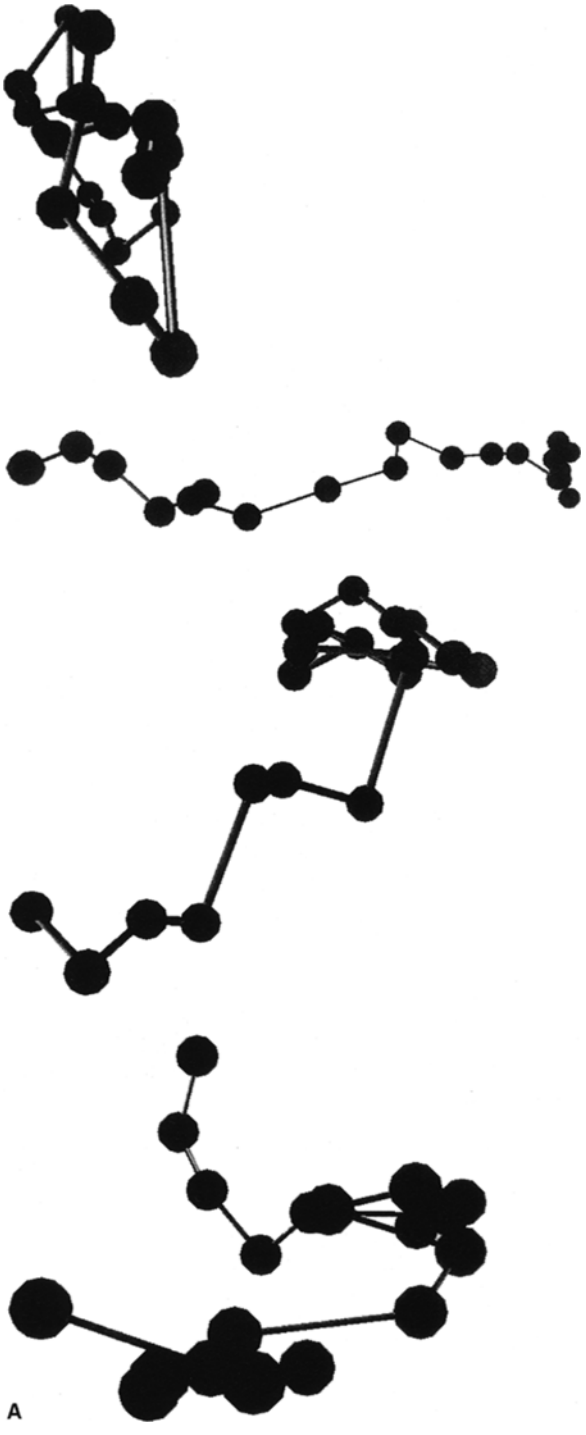

Fig. 9A Pictures of a polystyrene chain model at various stages in its trajectory through the simulated device. Volumetric flow rate used was $Q = 0.2\ cm^3/s$. The chain did not fracture with this flow rate. The molecular weight of the chain was 2.0×10^6. Hydrodynamic interaction was included (nonfree draining case). 1: At the start of the simulation. 2: Just in front of orifice ($x = -0.01$ cm). Chain extension reduced to fit on page 3: Just inside the orifice ($x = 0.01$ cm). 4: Inside the capillary ($x = 0.05$ cm)

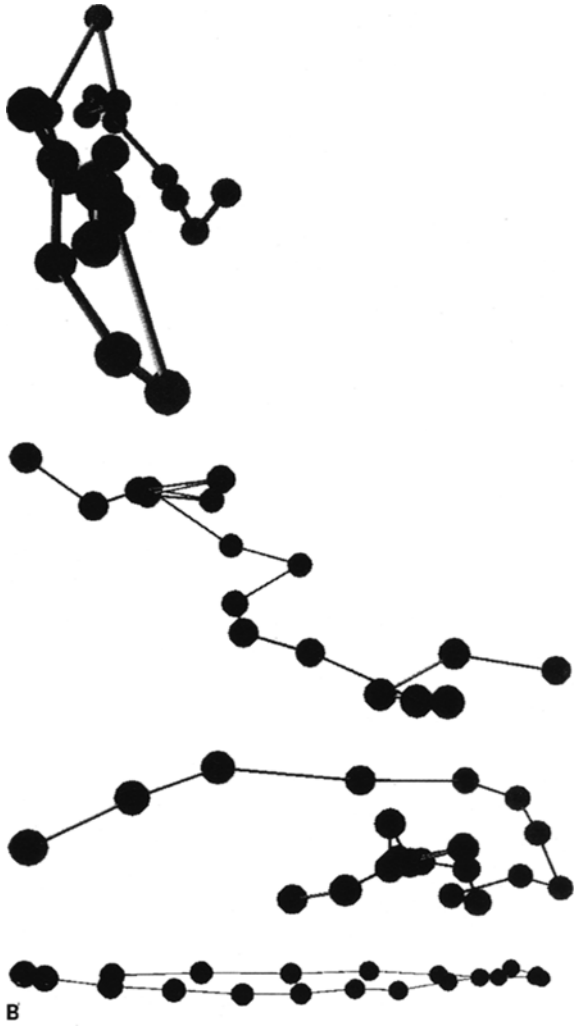

Fig. 9B Pictures of a polystyrene chain model at various stages in its trajectory through the simulated device. Volumetric flow rate used was $Q = 10.0\ cm^3/s$. The chain fractured with this flow rate. The molecular weight of the intact chain was 2.0×10^6

and 6A. However, as was shown by the fragment distribution in the non-free draining case (Fig. 8), this propensity for mid-chain folding is less when hydrodynamic interaction between the beads in the chain is taken into account (a situation that should correspond more to the laboratory experiment), resulting in a molecular weight distribution centered more around half of the initial molecular weight.

In the Method section, we describe the applied FENE model of polystyrene, having a maximum extension q_o around 10 (relative to the spring equilibrium length), obtained by forcing the ratio between critical extension for fracture q_c close to q_o ($q_c/q_o = 0.93$). We will now use a different approach, looking at the dimensions of the building blocks of polystyrene, to see if this value of q_o is reasonable. The chemical formula of the polystyrene

molecule can be written in shortform $[-CH-CH_2]n$ (the R-group of the first carbon atom is not shown here). Assuming standard C–C bond length equal to 1.54 Å, and tetrahedron angle of 109.4°, each monomer will present an axial length of 2.50 Å. Since the molecular weight of the polystyrene monomer equals 104.16 D, the length per Dalton will be 0.024 Å, from which we can finally find the maximum axial length in the stretched-out state (L_m) of polystyrene with molecular weight 2×10^6, giving $L_m = 4.81$ μm. Since, while using the bead-spring model for the polystyrene molecule, this length also must be equal to $(N-1)q_o$, N being the number of beads and q_o the maximum extension of each spring, we then find for the case that $N = 20$ (corresponds to $M = 2 \times 10^6$), that $q_o = 2530$ Å. Now, since we found while parameterizing our model (see Method section) that the equilibrium length, b, of a spring equals 217 Å, the relation between the maximum and equilibrium spring extension can finally be calculated as $q_o/b = 11.6$. This is not far from the value that was applied in the method section for the FENE-spring model of the polystyrene ($q_o/b = 8.8$), showing that the model that we used, where the intention was to preserve the FENE characteristics, was reasonable.

The use of FENE springs to represent subchains, rather than Gaussian springs employed in previous works [15, 16] is one of the main features of this study. We note that the critical scaling exponent found for the two models are quite similar. However, the two models store energy in quite different ways and amounts, and the elongational or flow rate required to break a chain may also be quite different. Therefore, for a quantitative prediction of the outcome of real experiments the more realistic FENE chain should be the choice.

With regard to the dissociation energy of the C–C bond, the value used (144 kcal/mol) may be questionable. In a polystyrene chain it is possible that the energy is somewhat lower [24]. However, the scaling laws and the qualitative aspects of the fracture process, which were the main aims of the present study, will probably not be affected by this difference.

Concluding remarks

In this study our aim has been to simulate the behavior of polystyrene molecules while subjected to an extensional flow of transient character, simulating a polymer/solvent system and an experimental device that has been employed in the laboratory of other authors, and trying to get more information about the differences that have been found to exist between stagnant and transient flow with respect to fracture of flexible polymer chains.

We observed fracture that depended strongly on flow rate and on molecular weight, with a critical flow rate for chain scission that was related to the molecular weight as $Q_{crit} \sim M^{-1.03}$. This scaling law is very different from that known to exist in *stagnant* extensional flow (exponent equal to -2.0), but corresponds well with theoretical predictions about the relation between molecular weight and critical flow rate in *transient* extensional flow (exponent equal to -1.0). We also observed that the scaling law was very different in the free-draining and the nonfree draining cases, illustrating the importance of taking into account hydrodynamic interaction in studies with transient extensional flow.

Acknowledgements We acknowledge the support from grants PB93-1132 (DGCYT-MEC), PIB94-07 (DGUI-CARM). K.D.K. acknowledges grant ERBCHBICT 940974 from the Commission of the European Communities.

References

1. Keller A, Odell JA (1985) Colloid and Polymer Sci 263:181
2. Muller AJ, Odell JA, Keller A (1988) J Non-Newt Fluid Mech 30:99
3. Odell JA, Keller A, Muller A (1992) J Colloid and Polymer Sci 270:307
4. Cathey CA, Fuller GG (1990) J Non-Newt Fluid Mech 34:63
5. Lopez Cascales JJ, García de la Torre J (1991) J Chem Phys 95:9384
6. Lopez Cascales JJ, García de la Torre J (1992) J Chem Phys 97:4549
7. Wiest JM, Wedgewood LE, Byron Bird R (1989) J Chem Phys 90:587
8. Larson RG, Magda JJ (1989) Macromolecules 22:3004
9. Odell JA, Keller A, Rabin Y (1988) J Chem Phys 88:4022
10. Nguyen TQ, Kausch H-H (1988) J Non-Newt Fluid Mech 30:125
11. Nguyen TQ, Kausch H-H (1990) Macromolecules 23:5137
12. Reese BH, Zimm BH (1990) J Chem Phys (1990) 92:2650
13. Rabin Y (1988) J Chem Phys 86:5215
14. Rabin Y (1988) J Non-Newt Fluid Mech 30:119
15. Knudsen KD, Hernández Cifre JG, García de la Torre J (1996) Macromolecules 29, in press
16. Knudsen KD, Hernández Cifre JG, López Cascales JJ, García de la Torre J (1995) Macromolecules 28:4660
17. Bird RB, Curtiss CF, Armstrong RC, Hassager O (1987) Dynamics of Polymeric Liquids. Vol 2. Kinetic Theory, Wiley, New York
18. Handbook of Chemistry and Physics (1972) CRC Press, Cleveland, Ohio
19. Schmidt M, Burchard W (1981) Macromolecules 14:210
20. Huber K, Bantle S, Lutz P, Burchard W (1985) Macromolecules 18:1461
21. Ermak DL, McCammon JA (1978) J Chem Phys 69:1352
22. Iniesta A, García de la Torre J (1990) J Chem Phys 92:2015
23. Yamakawa H (1970) J Chem Phys 53:436
24. Odell JA, Keller A (1986) J Polymer Sci 24:1889